Journal of Micro-Bio Robotics (2020) 16:215–224
https://doi.org/10.1007/s12213-020-00136-1

RESEARCH PAPER

Independent control of multiple magnetic microrobots: design, dynamic modelling, and control

Ruhollah Khalesi [1] · Hossein Nejat Pishkenari [1] · Gholamreza Vossoughi [2]

Received: 30 November 2019 / Revised: 8 May 2020 / Accepted: 5 June 2020 / Published online: 27 June 2020

Abstract

Swimming microrobots have a variety of applications including drug delivery, sensing, and artificial fertilization. Their small size makes onboard actuation very hard, and therefore an external source such as the magnetic field is a practical way to steer and move the robot. In this paper, we have designed a novel microrobot steered by magnetic paddles. We have also discussed design parameters where, based on the conducted simulation, the robot speed reaches 520 um/s. It is shown that the microrobot speed depends on the robot paddle dimensions. According to the microrobots motion characteristics and their different reactions to the same input, we have designed a steering strategy for point-to-point control of multiple microrobots.

Keywords Swimming microrobot · Magnetic field · Paddle · Low Reynolds number · Simultaneous control

1 Introduction

Microrobots by accessing small spaces have great potential in cell sorting, micro-assembly, drug delivery, and sensor networks [1–6]. Due to low speed and small size of microrobots, Reynold's number is very small, making inertial forces negligible in comparison with viscous forces. In this steady creeping flow, named Stokes flow, based on the Scallop theorem proposed by Purcell, in order to have a net displacement, the microswimmers must have nonreciprocal motion [7].

Due to small size of microrobots, design and fabrication of small onboard actuators and sensors are difficult tasks, but in literature, some works are based on using small-scale motors and actuators. In [6], Yang reviewed MEMS-based actuation and sensing methods. Actuators presented in this state-of-the-art survey, are listed in five main sub-groups: electro-thermal, electrostatic, shape memory alloy, piezoelectric, and electromagnetic actuators. In [8], using a global magnetic field and local magnetic interactions between two microgrippers, independent simultaneous position control of two microrobots with end-effectors were proposed. The global magnetic field also was employed for a gripper grasping and releasing command.

Jalali et al. [9] designed and simulated the motion of microswimmer named Quadroar composed of one linear and four rotary actuators. They proved this microrobot could perform three-dimensional reorientation and forward and transverse movement. In [10], orbital topology of two nearby swimming Quadroar is studied. They also showed that the hydrodynamic effect of two interacting swimmers leads to faster movement, but no experimental test was presented to validate the result. In [11], they designed, fabricated, and tested mm-scale Quadroar swimmer with silicone oil as the surrounding fluid to satisfy the low Reynolds number condition. They claimed theoretical and experimental results matched well. However, the fabrication of micro-scale actuators is not conventional by now; hence employing external actuation signals is a more practical solution.

The inspiration from nature is a customary technique in science. In nature, microorganisms use flagella or cilia for swimming. Flagella is a long thin organ, which generates force by bending or rotating. Cilia is shorter versus flagella but larger in quantity [12]. Each microorganism produces necessary force in each segment internally. However, due to the

Electronic supplementary material The online version of this article (https://doi.org/10.1007/s12213-020-00136-1) contains supplementary material, which is available to authorized users.

✉ Hossein Nejat Pishkenari
nejat@sharif.edu

[1] Nanorobotics Laboratory, Department of Mechanical Engineering, Sharif University of Technology, Tehran, Iran

[2] Department of Mechanical Engineering, Sharif University of Technology, Tehran, Iran

small size of microrobots, they cannot carry power sources, sophisticated actuators and sensors, so simple designs are needed which are based on external energy sources.

There are many different mechanisms to actuate microrobots such as laser beam, physiological energy, electrics field, acoustic field, thermal energy, light, and magnetic field [13, 14]. Using an external magnetic field is the first choice in many cases because it can penetrate different materials, is not harmful to the body, and can generate force and torque quickly. Magnetic field-based driving modes are classified into three main subgroups: rotating field, oscillating fields, and field gradients [12].

Using magnetotactic bacteria for targeted cell killing was investigated in [15]. First, they moved microrobots to a target location using a gradient magnetic field. Then, by generating a rotating field, microrobots were mixed with target cells and, finally, by swinging field, target cells were killed. This procedure prevented real-time monitoring difficulties.

In [16], a microrobot based on artificial bacterial flagella, capable of swimming using a rotating magnetic field was presented. This microrobot consists of a helical tail and a soft magnetic metal head. Three orthogonal electromagnetic coil pairs generate a rotating magnetic field leading to propulsion and steering of the microrobot in water.

As mentioned, the microorganism can generate force and torque in each segment of their cilia. In [17], a microrobot named ParaLiker with a similar assumption was proposed, and dynamic model and equations of motion were derived. This microrobot with 500 cilia has a maximum speed of 4 mm/s and an efficiency of 40%. Inspiring from a sperm cell, in [18], a microrobot with a flexible tail and magnetic head was proposed, which moves by an external oscillating magnetic field. The average speed was about 160 μm/s, and its controllability and steering were experimentally verified.

In [19], a microrobot was designed, fabricated, and manipulated by an externally applied stepping magnetic field. The magnetic force was calculated as a function of magnetic field strength, field angle, cilia length, angle, etc. In addition, the position and orientation of the microrobots were controlled, and particle displacement was demonstrated experimentally. In [20], a theoretical model for artificial cilium was proposed and using analytical calculation and numerical simulation, dynamic properties were investigated. This microrobot was moved using a rotating magnetic field. Besides, in [21], a theoretical model of microrobot with two flagella was developed, and the motion in bulk fluid and close to a solid surface were investigated using numerical simulation.

Using multiple robots can improve speed and functionality. Independent control can also increase the total performance of a robotic system including several robots. There are two main approaches to control multiple robots simultaneously by a magnetic system. First, generating different magnetic fields and gradients in the workspace in a way that each microrobot experiences a distinct magnetic field and gradient. Therefore, each microrobot receives specific force and torque and tracks its desired path. However, since the distance among microrobots is very small, generating distinct fields at robot locations is not an easy task [14]. The second method of controlling multiple robots is generating a uniform field or gradient in space and using non-identical microrobots in order to control their motion independently [22]. In this case, the robots can differ magnetically, geometrically, electrically, or thermally.

Simultaneous control of multiple microrobots has been widely studied in recent years. Ref [22] summarized different approaches and discussed challenges. In [23], Sitti et al. used electrostatic anchoring pads to control two microrobots in both uncoupled individual motion and coupled symmetric motion. Pads work as a brake and stop the desired microrobot from moving in the field gradient direction. This approach is limited to a 2D movement and needs special surfaces.

Controlling identical microrobots, is a difficult task. Kumar et al. [24], proposed a force control method based on varying gradient with stationary electromagnetic coils. They numerically simulated concurrent control of two microrobots and validated results in the macroscopic experiments. In [25], Misra et al. designed and tested electromagnetic setup for independent 3D control of two identical and non-identical microrobots. The setup consists of nine electromagnetic coils, and 6-DOF independent navigation was evaluated.

In [26], Diller et al. proposed methods for simultaneous control of mag-μBots that were geometrically different. In addition, they investigated control strategies, and in an experiment, independent global positioning of two and three microrobots in 2D was demonstrated.

Nelson et al. controlled two helical microrobots using a rotating magnetic field and moved micro bars by large propulsive force [27]. They also showed that these microrobots could manipulate micro-objects either by direct contact or through the fluid motion generated by their rotation. They also showed that even though these tasks can be done by single microrobot, but challenges in precise manipulation, increment in operation time, and limitations of the size and the weight of the cargo must be considered.

Cheang et al. controlled untethered microrobots, which are geometrically similar but magnetically different, using a single rotating magnetic field. Their different magnetic properties led to different swimming behaviors by controlling the strength and frequency of the field [28]. In [29] Kumar et al., presented a method for open-loop control of multiple catalytic microrobots. In this approach, the directions of motion were regulated by catalytic cap and different trajectories were tracked by microrobots. They used a simple model to validate strategy experimentally.

As mentioned, generating different magnetic fields in a small workspace is a challenging issue. Therefore, in order

to control microrobots independently, we need non-identical robots, but manufacturing sophisticated designs needs special devices and small-scale actuators. In this work, we propose a design that uses cilia and a disk like a paddle to produce a difference in microrobots and improve functionality and speed. Cilia as a moving mechanism is widely used in many papers, and a similar mechanism for rotating parts was proposed and fabricated in [30] using 3-D laser direct writing, so fabrication of cilium and a rotating disk without a motor is a practical concept. A combination of these two approaches extends design options, which can be adjusted to improve speed and simultaneous control capability of microrobots.

Figure 1 depicts a schematic view of the proposed paddle. We consider the magnetization vector of the cilia and the disk in the specific direction in order to prevent reciprocal motion and generate proper movement. These directions are shown in this figure. The microrobot has several cilia, and each cilium has a magnetic disk on its free end. Disks can rotate freely but limited about their axis of connection, and by applying a periodic magnetic field, disks will rotate, and cilium will bend with different time constants. The rotation direction does not affect moving ability and disks can rotate clockwise or counter clockwise. But, the range of rotation is an important factor and should be restricted to generate net displacement. If the rotation angle has not been limited around zero, in the recovery phase the disk will rotate to −85 degree and, the effective area will be maximized in this phase too which prevents from net motion of the robot. So, limiting the rotation angle will force the disk angle to be 5 degree during recovery phase and the effective area will be minimized.

As it is shown in Fig.1, the disk and cilium magnetization directions are different. It should be noted that practical implementation of unaligned magnetization of the disk and the cilia may be challenging. To address this problem, we can magnetize both the disk and the cilia in the same direction,

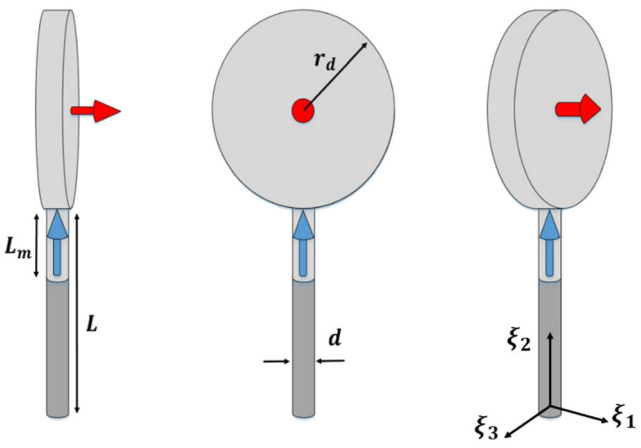

Fig. 1 Front and side views of paddle, red arrows are magnetization vectors of the disk and the blue ones are magnetization vectors of the cilia. Radius of the disk (r_d), diameter of the cilia (d), total length (L) and magnetized length (L_m) of the cilium are shown

which is the mean direction of plotted vectors in the figure. As it will be shown later on in this paper, in this situation the mechanism retains its functionality with less efficiency but it would be more feasible with the current technology. In order to keep the symmetry, cilia are placed around the microrobots. So, magnetization process should be started to bend the cilia and continued until all the cilia and the disks achieve the same magnetization vector. However, in simulations magnetization vectors are assumed as Fig. 1. In section D effect of this assumption is investigated.

Figure. 2 shows the microrobot design. Parts (a) and (b) show schematic of the microrobots and reference axis which is used in this paper and, part (c) presents the concepts of the motion. The first cilium is in its initial condition (90 degrees) and an external magnetic field, in the negative x direction, is applied to bend the cilia to the beginning of the propulsive phase. Then, a periodic external magnetic field is applied to generate motion.

In the propulsion phase, the external magnetic field is applied in the x-direction, which will cause bending of the cilium and rotation of disks, so disks will stand normal versus the moving direction in the majority of the phase.

On the contrary, in the recovery phase, the external magnetic field applied in the negative direction of the x-axis. So, cilia will be bend in the same direction, and disks will rotate to align with the external magnetic field direction, but as the rotation angle is limited physically, they will be parallel versus the moving direction in the majority of the period. The difference between these two phases generates net displacement (Fig. 2-c). In order to prevent disks from locking, their rotation angles have been limited from 5 to 85 degrees.

It must be noted that in the beginning of oscillation cycles, cilium does not have a steady response to the external magnetic field and the range of bending angle changes. But after elapsing some cycles from motion, cilium will reach to its steady state response and shows a periodic oscillation. The range of bending angle in the steady-state condition is determined by the frequency of the external magnetic field and the physical and geometrical parameters of the cilium.

Therefore, the proposed design uses several paddles, which are a combination of artificial cilia with a disk in its end. The external magnetic field bends the cilia and rotates the disk, and changing the direction of this field leads to paddling.

2 Microrobot design

In microscale systems, due to low Reynolds number, the viscous forces are dominant, and the inertial forces play a small role. As a result, Navier-Stokes equations are simplified to Stokes equations as follows [17].

$$\nabla \mathrm{p} = \mu \nabla^2 \mathbf{u}, \nabla . \mathbf{u} = 0 \quad (1)$$

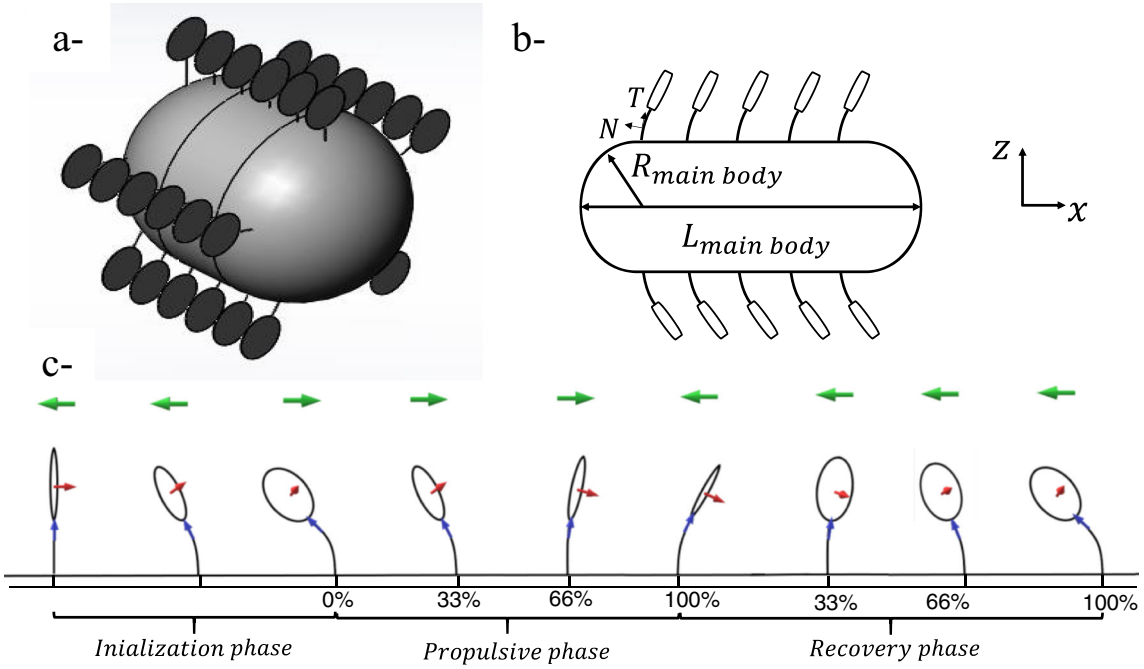

Fig. 2 **a**- Isometric view of microrobot **b**- Simplified top view of microrobot and body coordinate **c**- Cilia's sequence of motion (green arrows show the external magnetic field direction, and blue and red arrows show cilia and disk magnetization vectors in different time instants. Percentages show the elapsed time of each phase).

Where p and μ are pressure and dynamic viscosity of the fluid, and **u** is the fluid velocity. Force and torque exerted by a magnetic field on the magnetic object can be expressed as:

$$\mathbf{F_m} = (\mathbf{m}.\nabla)\mathbf{B} \tag{2}$$

$$\boldsymbol{\tau_m} = \mathbf{m} \times \mathbf{B} \tag{3}$$

Here $\mathbf{F_m}$,$\mathbf{m}$,$\mathbf{B}$, and $\boldsymbol{\tau_m}$ are respectively magnetic force, the magnetic dipole moment of the object, external magnetic field, and magnetic torque vectors.

2.1 Hydrodynamics of cilia

Magnetized cilia is bent by the external magnetic field, which leads to a drag force proportional to velocity and in the opposite direction. This force in tangential and normal directions is approximated as

$$\phi_T(s,t) = -C_T V_T(s,t) \tag{4}$$

$$\phi_N(s,t) = -C_N V_N(s,t) \tag{5}$$

Where ϕ, C, and V are drag force, resistance coefficient and velocity and subscripts T and N denote tangential and normal directions versus cilia (Fig. 2.b), s and t are arc length parameter and time respectively.

Tangential and normal resistance coefficients are approximated as [17].

$$C_T = \frac{8\pi\mu}{-2 + 4\ln\left(4q/d\right)} \tag{6}$$

$$C_N = \frac{8\pi\mu}{1 + 2\ln\left(4q/d\right)} \tag{7}$$

In the above equations d and q are cilium diameter and arbitrary value provided that $q << L$ and $d << q$. L is the length of cilia.

It is assumed that cilium is as an inextensible part, and α(s, t) is the angle between point s and x-axis. Using geometrical constraints to calculate velocities yields [31]:

$$\frac{\partial V_N}{\partial s} = \frac{\partial \alpha}{\partial t} - V_T \frac{\partial \alpha}{\partial s} \tag{8}$$

$$\frac{\partial V_T}{\partial s} = V_N \frac{\partial \alpha}{\partial s} \tag{9}$$

In addition, by considering Newton and Euler equations of motion, we have [31]:

$$\frac{\partial F_T}{\partial s} - F_N \frac{\partial \alpha}{\partial s} = \phi_T \tag{10}$$

$$\frac{\partial F_N}{\partial s} + F_T \frac{\partial \alpha}{\partial s} = \phi_N \tag{11}$$

$$\frac{\partial M}{\partial s} = F_N \tag{12}$$

Where F and M are internal force and moment of the cilium. If cilium is considered as a beam, the bending moment can be substituted by $EI\frac{\partial\alpha}{\partial s}$ and from Eq. (12) we have

$$F_N = EI\frac{\partial^2\alpha}{\partial s^2} + \frac{\partial M_{emf}}{\partial s} \tag{13}$$

In above equation M_{emf} is the external magnetic field moment on the magnetized part of the cilium. The first part of the right-hand side of Eq. (13) states the effect of elasticity of cilia, and the second one is a force produced by the external magnetic field. Finally combining geometrical constrains and force constraint we have:

$$\frac{\partial^2 F_T}{\partial s^2} = \left(1+\frac{C_T}{C_N}\right)\frac{\partial F_N}{\partial s}\frac{\partial\alpha}{\partial s} + \frac{C_T}{C_N}F_T\left(\frac{\partial\alpha}{\partial s}\right)^2 + F_N\frac{\partial^2\alpha}{\partial s^2} \tag{14}$$

$$\frac{\partial^2 F_N}{\partial s^2} + \left(1+\frac{C_N}{C_T}\right)\frac{\partial F_T}{\partial s}\frac{\partial\alpha}{\partial s} + F_T\frac{\partial^2\alpha}{\partial s^2} + C_N\frac{\partial\alpha}{\partial t} = \frac{C_N}{C_T}F_N\left(\frac{\partial\alpha}{\partial s}\right)^2 \tag{15}$$

Equations (13), (14), and (15) are three PDE including nonlinear terms, which couples the elastic, hydrodynamic, and magnetic forces and should be solved numerically. At each time step, F_N is calculated using Eq.(13) and previous step cilium shape, then F_T is obtained from Eq. (14), and finally, $\frac{\partial\alpha}{\partial t}$ is determined based on Eq. (15). Thereby the velocity of cilia and drag forces can be computed (for more details see [31]).

2.2 Hydrodynamics of disk

Drag force on moving disk in a fluid is a function of drag coefficient, fluid viscosity, and relative velocity.

Drag force and torque on disk are calculated as [9]:

$$\mathbf{F_{disk}} = -\mu[\mathbf{K}]\mathbf{u} \tag{16}$$

$$[\mathbf{K}] = \frac{16}{3}r_d\left(3\hat{\mathbf{i}}_1\otimes\hat{\mathbf{i}}_1 + 2\hat{\mathbf{i}}_2\otimes\hat{\mathbf{i}}_2 + 2\hat{\mathbf{i}}_3\otimes\hat{\mathbf{i}}_3\right) \tag{17}$$

$$\boldsymbol{\tau}_{\mathbf{disk}} = -\mu[\mathbf{Q}]\boldsymbol{\omega} \tag{18}$$

$$[\mathbf{Q}] = \frac{32}{3}r_d^3\mathbf{I} \tag{19}$$

In above equations, $\mathbf{F}_{disk}$, $\boldsymbol{\tau}_{disk}$, $[\mathbf{K}]$ and $[\mathbf{Q}]$ are drag force and torque on the disk, and drag coefficient matrices. In Eq.(17), r_d is radius of the disk and $\hat{\mathbf{i}}_j$ (j = 1, 2, 3) is a reference coordinate unit vector.

If we write Euler equation of motion for a rotating disk and ignore inertial terms, we have

$$\sum\boldsymbol{\tau} = 0 \rightarrow \boldsymbol{\tau}_{\mathbf{m}} + \boldsymbol{\tau}_{\mathbf{disk}} + \boldsymbol{\tau}_{\mathbf{f}} = 0 \tag{20}$$

Where $\boldsymbol{\tau}_{\mathbf{f}}$ is the friction torque in the joint. By applying the magnetic field, the disk begins to rotate and eventually reach an equilibrium angle. To obtain the angle of the disk at any moment, it is necessary to solve the above equation. The rotation time constant of the disk is a function of its magnetization, and geometrical parameter of the disk and the joint. Therefore, by changing these parameters, the time constant of rotation rate can be adjusted. In the conducted simulations, a value will be assumed for the time constant of rotation appeared in this equation, and the angle of the disk is assumed to be known by this parameter.

2.3 Equations of Motion

Based on equations introduced in subsections A and B, the velocity of each point of cilium can be calculated and then drag forces are approximated as

$$\phi_T(s,t) = -C_T(V_T - U\cos\alpha) \tag{21}$$

$$\phi_N(s,t) = -C_N(V_N + U\sin\alpha) \tag{22}$$

Then using the following equations, the force on element ds by neglecting inertial forces is as follows

$$dF_{x,cilium} = (-\phi_T\cos\alpha + \phi_N\sin\alpha)ds \tag{23}$$

$$dF_{y,cilium} = (\phi_N\cos\alpha + \phi_T\sin\alpha)ds \tag{24}$$

Based on the symmetry of cilia, force in the y-direction vanishes and the main force is computed as follow

$$dF_{x,cilium} = \left(C_TV_T\cos\alpha - C_TU\cos^2\alpha - C_NV_N\sin\alpha - C_NU\sin^2\alpha\right)ds \tag{25}$$

Finally, by integrating this force along the length of the cilium, the total external force exerted on the cilium in the x-direction is

$$F_{x,cilia} = N\int dF_{x,cilium} \tag{26}$$

Where, N is the number of cilia. It should be noted that in numerical simulation, for the boundary condition of PDE, the cilium is considered to be fixed in one end, and the external magnetic force and moment exerted through disk are applied on the other cilia end. Drag force exerted on the main body is calculated as [17]:

$$F_{x,main} = 8.5\mu r_m U \tag{27}$$

Where, r_m is the effective radius of the main body. By neglecting the inertial force which is much lower than the drag forces, the force equation for the microrobot can be given as:

$$\sum\mathbf{F} = 0 \rightarrow F_{x,cilia} + F_{x,disk} + F_{x,main} = 0 \tag{28}$$

As a result, the velocity of the microrobot can be found as:

$$U = \frac{\sum F_{x,cilia} + F_{x,disk}}{8.5\mu r} \tag{29}$$

Paddles are symmetrically distributed on the main body of the microrobot, which will cause forces only exert in the x-direction theoretically, and the forces in other directions vanish.

2.4 Numerical simulation

To demonstrate the performance of the proposed microrobot, we have conducted some numerical simulations. A microswimmer with forty cilia, N = 40, is investigated in our simulation. Table 1 shows the microrobot specifications (cilia physical parameters are similar to [17]). The fluid viscosity is considered to be $0.001 m^2/s$.

Each cilium is divided into 50 segments, and a system of nonlinear partial differential equations are solved for each part by applying a zero-velocity boundary condition in infinity and no-slip boundary condition at the cilia outer surface.

A periodic square wave magnetic field with amplitude seven milli tesla, a 50% duty cycle (with equal positive and negative pulse width), and frequency 0.7 Hz is applied in x-direction. During the effective stroke, cilia bends from the initial angle of 130^0 to 100^0 and, at recovery stroke, it returns to its initial angle. As mentioned before, a disk is connected to cilium by joint, and the time constant of rotation can be regulated. In this simulation, the time constant of disk's rotation is considered as 0.2 s. The results in this section are for the steady-state condition and initial periods of the motion are ignored.

Drag force on disk, angle of cilium's end, the rotation angle of the disk, and position of the micro robot (integral of the speed of the microrobot) are shown in Fig. 3. The rotation angle of the disk changes its effective area and, consequently its drag force. This is the main reason that generates net displacement in each cycle. The mean value of speed in each cycle is reported as a net speed, and in this condition, this value is 13 μm/s. It must be noted that by increasing the number of the cilium, higher speed is achievable. For the microrobot considered here with 40 cilia, the microrobot mean speed will be 520 μm/s.

Table 1 Microrobot specifications

parameter	unit	Value
Number of cilia	–	40
Length of cilium	μm	15
Radius of cilium	nm	12.5
Magnetized length of cilium	μm	4.5
Radius of main body	μm	150
Length of main body	μm	400
Radius of disk	μm	35
Cilium magnetization	A. mm^2	10^{-4}
Cilia Elasticity module	GPa	5

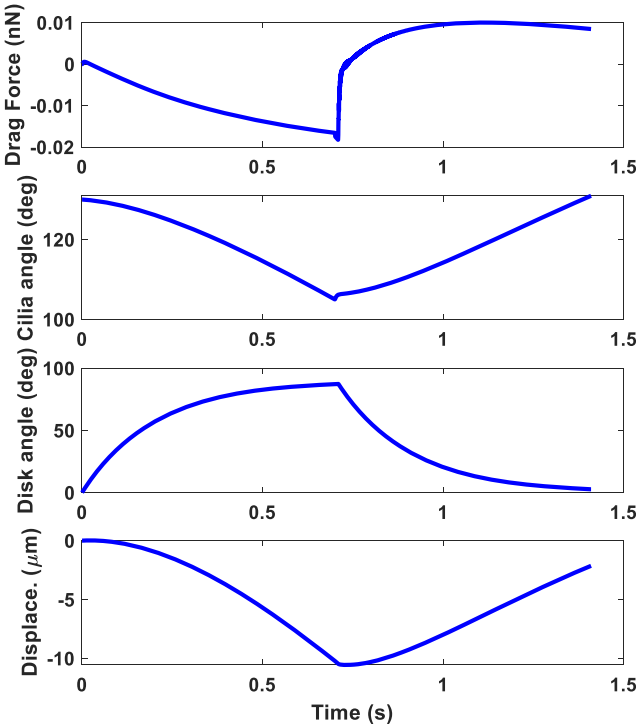

Fig. 3 Drag force on the disk, the cilium bending angle, the disk rotation angle and displacement of the microrobot in one complete cycle of the external magnetic field

Cilia bending in the propulsive and recovery strokes are shown in Fig. 4 As can be seen after one complete cycle, cilium returns to its initial orientation. In presented design, distance between two consecutive cilia is about 5 μm. Thus, the magnitude of the magnetic field generated by a cilium near its neighbor is about 0.16 milliTesla which is about 2% of the external magnetic field and magnetic interaction among the cilia can be ignored.

If the disk and cilia have a similar magnetization direction, and β is defined as an angle between this magnetization vector and the vertical line (ξ_2-axis in Fig. 1), the microrobot motion

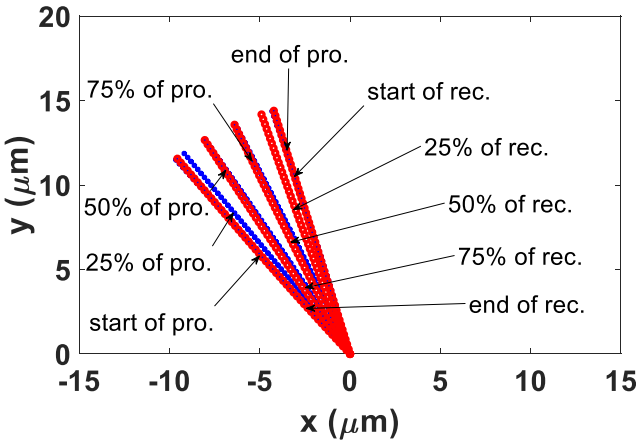

Fig. 4 Cilium in propulsive (*/blue) and recovery (o/red) phases

Table 2 Microrobot mean speed versus the magnetization direction angle

β (degree)	Mean speed ($^{\mu m}/_{s}$)
15	10.21
30	6.16
45	1.53

for different values of β can be simulated. Table 2 lists the microrobot mean speed for 4 different values of β. For these simulations disk rotation time constant is assumed to be 0.2 s for all the presented diagrams. As it is shown, in this situation the microrobot moves with lower speed but the robot mechanism is more feasible with the current technology. It should be note that in the current design which is based on different magnetization directions for cilia and disk, the micro robot mean speed is 13.13 (μm/s). By aligning the magnetization direction for the disk and cilia, the efficiency has decreased. This can be seen in the reduction of the average speed but the movement mechanism still works.

Now we return to our primary assumption which was different magnetization directions for the disk and cilia. Figure 5 shows how average speed of the microrobot changes with its geometrical parameters. Except for the values shown, the other parameters are the same as Table 1. By increasing the main body radius, the drag force on the microrobot increases, which yields a slower speed. The microrobot moves based on disks drag force, so increasing disk radius will lead to an increase of speed.

As cilia becomes thicker, flexural stiffness and bending time constant of cilia will increase, and disks move by their most effective area for a longer period. However, it will cause a smaller sweeping area that has a negative effect on the speed. In the first half of the plot where R < 12 nm, the first reason has a stronger effect while in the next half the second reason is dominant. An increase in the length of cilia has a dual effect too. Firstly, it will provide more flexibility and easier cilia bending. Hence, the cilia time constant and mean speed reduces. Secondly, the velocity of disks based on cilia bending will increase, which yields to increase of the microrobot speed. As can be seen, the first effect is dominant.

Figure 6 displays how the microrobot mean speed varies with magnetization and elasticity. By increasing the external magnetic field strength, the cilium magnetization, or the cilium magnetized length, the magnetic force increases, which yields to a higher speed of microrobot. Increment in the module of elasticity decreases bending time constant and increases the speed of the microrobot.

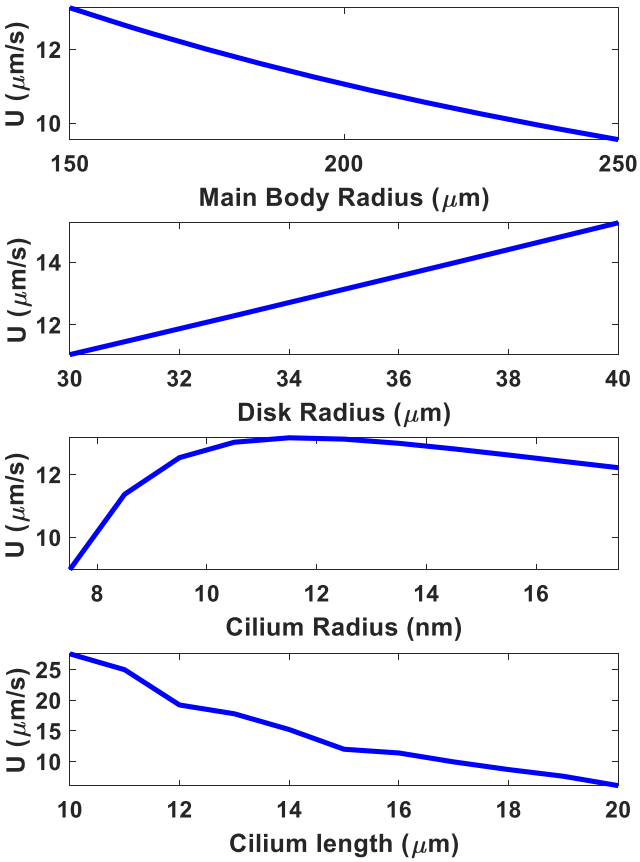

Fig. 5 Mean speed of the microrobot versus radius of the main body, disk radius, the cilia radius and the cilium length

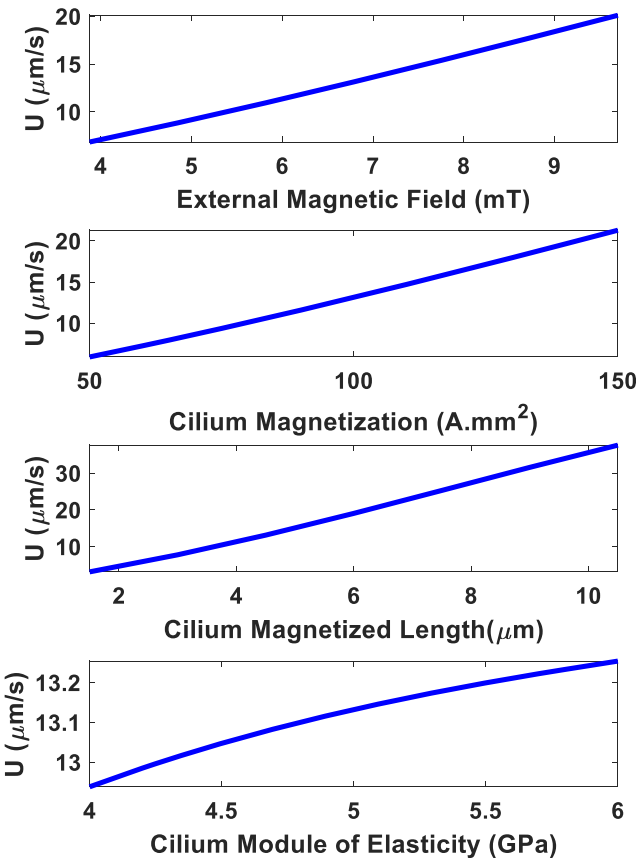

Fig. 6 Mean speed of the microrobot versus the external magnetic field, cilium magnetization strength and length, and module of elasticity

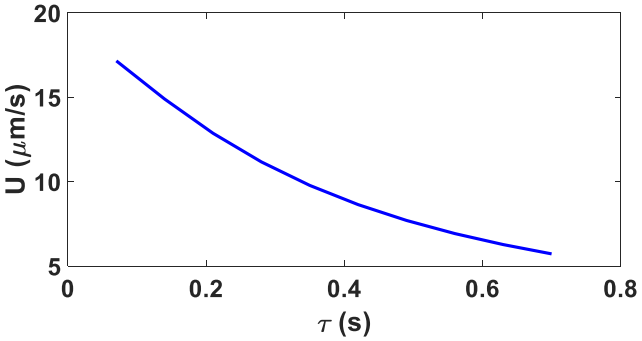

Fig. 7 Mean speed of the microrobot versus the time constant of the disk rotation

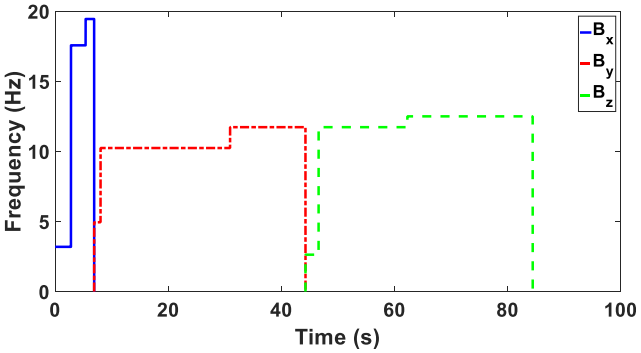

Fig. 9 External magnetic field frequency

If we repeat this simulation for different values of disk rotation time constants, it can be seen that by increasing the time constant, the net speed will be reduced because changes in the effective area will decrease (Fig. 7). According to the conducted simulations, the microrobot speed is a function of multiple parameters such as length and radius of cilia, the radius of disk and main body, magnetization parameters, etc. which can be optimized to maximize activation.

2.5 Simultaneous control of three microrobots

In this section, the ability to generate different speeds by an identical magnetic field will be used to independently control microrobots with different geometrical specifications. We focus on simultaneous control of three microrobots but the concept is similar for a higher number of microrobots. Figure 8 shows microrobots mean speed versus frequency of the external magnetic field for three microrobots. The disk rotation time constant for microrobots one to three are assumed as 0.02, 0.12, 0.08 respectively. For microrobots one and two, parameters are as same as Table 1. For microrobot three, only the magnetized length of the cilium and the radius of disks are different form the first two microrobots. These parameters for microrobot three, are set to 7.5 and 25 μm respectively.

We can see that these three microrobots have different reactions to similar inputs. As an example, if the frequency of the external magnetic field has been set more/less than12 Hz,

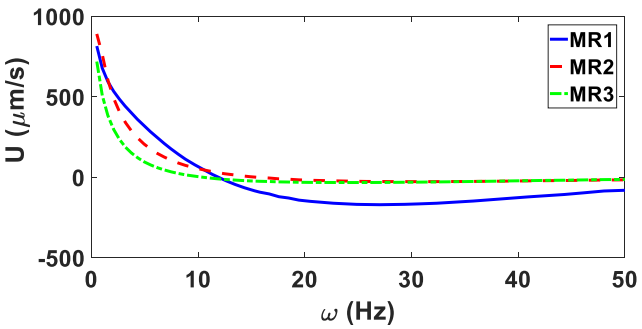

Fig. 8 Mean speed of the microrobot versus the frequency of the external magnetic field

the first one moves faster/slower than the second one. It must be noted that in higher frequency, the period of each phase is small and there is not enough time to fulfill disk rotation, so the effective area in two phases does not change a lot and the difference between cilia bending shapes in propulsive and recovery phases yield to negative velocity. Due to the constraints imposed by the cilia in the rotation of the disk, its effective area is a function of the disk rotation angle and the cilia end angle itself. So, in cases where the frequency is high and there is not enough time for complete disk rotation, the cilia angle plays a key role. In propulsive phase this angle is larger and, as a result, the effective cross-section is less and vice versa. However, the speed of the microrobot in this condition is very small due to semi-identical motions of cilia in propulsive and recovery phases. According to Fig. 8, the first microrobot with the lowest time constant reaches the negative moving velocity at a lower frequency.

This difference is used in independent control of microrobots. As the ratio of each two microrobot's speeds is not constant at different frequencies, the operator can choose the appropriate frequency based on trajectory defined. As this

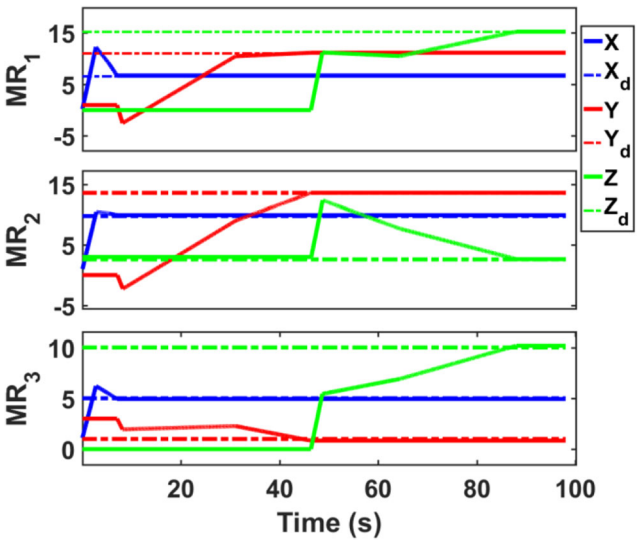

Fig. 10 Trajectory of microrobots (in mm) in simultaneous control

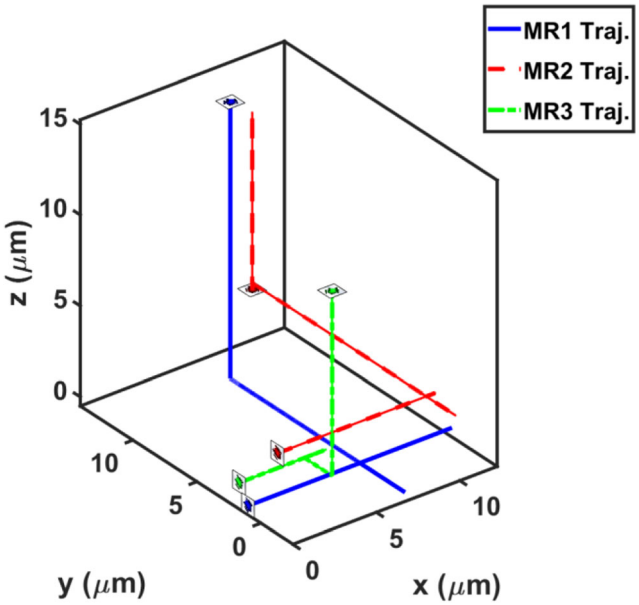

Fig. 11 Traveled trajectory of microrobots in independent control

ratio is limited to a small range of numbers, we need to separate each displacement into three parts, and the combination of movements leads to final desired displacements.

For example, assume three microrobots must move respectively e_1,e_2 and e_3 millimeter along the x-direction. We have

$$U_1(\omega_1)\frac{n}{\omega_1}+U_1(\omega_2)\frac{m}{\omega_2}+U_1(\omega_3)\frac{p}{\omega_3}=e_1 \quad (30)$$

$$U_2(\omega_1)\frac{n}{\omega_1}+U_2(\omega_2)\frac{m}{\omega_2}+U_2(\omega_3)\frac{p}{\omega_3}=e_2 \quad (31)$$

$$U_3(\omega_1)\frac{n}{\omega_1}+U_3(\omega_2)\frac{m}{\omega_2}+U_3(\omega_3)\frac{p}{\omega_3}=e_3 \quad (32)$$

Where U_i and ω_i (i = 1, 2, 3) are microrobots speed and phases frequency of the external magnetic field and, n, m and p are integer numbers to complete every cycle of fields implementation. By solving these linear equations, the control signals are calculated, and the solution with the shortest time is chosen.

For example, control signals and trajectories are shown in Figs. 9 and 10 for the case which first microrobot needs to move from [0,1,0] to [7, 11, 15] millimeter, the second one from [1,0,3] to [3, 10, 13] millimeters, and the last one from [1,3,0] to [1, 5, 10] millimeters.

At the first step, microrobots move in the *x*-direction by applying the external magnetic field for 2.80, 2.60, and 1.51 s respectively with frequencies 3.2, 17.6, and 19.4 Hz. The next step is applying magnetic field in the y-direction for 1.12, 22.90, and 13.32 s respectively with frequencies 4.9, 10.2, and 11.7 Hz. Finally, magnetic field is exerted in the z-direction for 2.32, 15.69, and 22.16 s respectively with frequencies 2.32, 15.69, and 22.16 Hz.

Figure 11 shows 3-dimensional trajectory of three microrobots. This is a simple point-to-point simultaneous independent control of three microrobots and the magnetic field is only exerted along the main axes of coordinate. As it noted, simultaneous control of more microrobots is possible with the similar concept only by increasing number of parts of each direction's movement.

3 Conclusion

In summary, we proposed a novel magnetic swimming microrobot with a new design, which uses magnetized disks and cilium actuated by external magnetic field. By applying the external magnetic field, cilium starts to bend. Also, disks rotate but with different time constant, which leads to a non-reciprocal motion. In the propulsive phase, disks will move perpendicular to the microrobot's x-axis, and their effective area against fluid are maximized. In the return stroke, disks will move parallel to the x-axis and it will minimize drag force. The proposed design with 40 cilia has a mean speed of 520 μm per second theoretically.

By changing design parameters such as cilium magnetized length and disk radius, microrobots reaction to the same input will be different, and this will lead to the ability of independent point-to-point control of multiple microrobots.

References

1. Kong L, Guan J, Pumera M (2018) Micro-and nanorobots based sensing and biosensing. Curr Opin Electrochem 10:174–182
2. Kim K, Guo J, Liang Z, Fan D (2018) Artificial micro/nanomachines for bioapplications: biochemical delivery and diagnostic sensing. Adv Funct Mater 28(25):1705867
3. Jeon S, Hoshiar AK, Kim K, Lee S, Kim E, Lee S, Kim JY, Nelson BJ, Cha HJ, Yi BJ, Choi H (2019) A magnetically controlled soft microrobot steering a guidewire in a three-dimensional phantom vascular network. Soft robotics 6(1):54–68
4. Pedram A, Nejat Pishkenari H (2017) Smart micro/nano-robotic systems for gene delivery. Current gene therapy 17(2):73–79
5. Le VH et al (2018) Preparation of tumor targeting cell-based microrobots carrying NIR light sensitive therapeutics manipulated by electromagnetic actuating system and Chemotaxis. Journal of Micro-Bio Robotics 14(3–4):69–77
6. Yang S, Xu Q (2017) A review on actuation and sensing techniques for MEMS-based microgrippers. Journal of Micro-Bio Robotics 13(1–4):1–14
7. Purcell EM (1977) Life at low Reynolds number. Am J Phys 45(1):3–11
8. Zhang, J, M Salehizadeh, and E Diller (2018). *Parallel pick and place using two independent untethered mobile magnetic microgrippers*. In *2018 IEEE International Conference on Robotics and Automation (ICRA)*. IEEE

9. Jalali, MA, M-R Alam, and S Mousavi (2014). *Quadroar: a versatile low-Reynolds-number swimmer*. arXiv preprint arXiv: 1408.5428
10. Mirzakhanloo M, Jalali MA, Alam M-R (2018) Hydrodynamic choreographies of microswimmers. Sci Rep 8(1):3670
11. Saadat, M, et al. (2019), *The experimental realization of an artificial low-reynolds-number swimmer with three-dimensional maneuverability*. arXiv preprint arXiv:1905.05893
12. Peyer KE, Zhang L, Nelson BJ (2013) Bio-inspired magnetic swimming microrobots for biomedical applications. Nanoscale 5(4): 1259–1272
13. Halder A, Sun Y (2019) *Biocompatible propulsion for biomedical micro/nano robotics*. Biosens Bioelectron 139:111334
14. Chen XZ, Jang B, Ahmed D, Hu C, de Marco C, Hoop M, Mushtaq F, Nelson BJ, Pané S (2018) Small-scale machines driven by external power sources. Adv Mater 30(15):1705061
15. Chen C, Chen L, Wang P, Wu LF, Song T (2019) Steering of magnetotactic bacterial microrobots by focusing magnetic field for targeted pathogen killing. J Magn Magn Mater 479:74–83
16. Zhang L, Abbott JJ, Dong L, Kratochvil BE, Bell D, Nelson BJ (2009) Artificial bacterial flagella: Fabrication and magnetic control. Appl Phys Lett 94(6):064107
17. Ghanbari A, Bahrami M, Nobari M (2011) Methodology for artificial microswimming using magnetic actuation. Phys Rev E 83(4): 046301
18. Khalil IS et al (2014) MagnetoSperm: a microrobot that navigates using weak magnetic fields. Appl Phys Lett 104(22):223701
19. Kim S, Lee S, Lee J, Nelson BJ, Zhang L, Choi H (2016) Fabrication and manipulation of ciliary microrobots with nonreciprocal magnetic actuation. Sci Rep 6:30713
20. Meng F, Matsunaga D, Yeomans JM, Golestanian R (2019) Magnetically-actuated artificial cilium: a simple theoretical model. Soft Matter 15(19):3864–3871
21. Shum H (2019) Microswimmer propulsion by two steadily rotating helical flagella. Micromachines 10(1):65
22. Chowdhury S, Jing W, Cappelleri DJ (2015) Controlling multiple microrobots: recent progress and future challenges. Journal of Micro-Bio Robotics 10(1–4):1–11
23. Pawashe C, Floyd S, Sitti M (2009) Multiple magnetic microrobot control using electrostatic anchoring. Appl Phys Lett 94(16): 164108
24. Wong D, Steager EB, Kumar V (2016) Independent control of identical magnetic robots in a plane. IEEE Robotics and Automation Letters 1(1):554–561
25. Ongaro F et al (2018) Design of an Electromagnetic Setup for independent three-dimensional control of pairs of identical and non-identical microrobots. IEEE Trans Robot 35(1):174–183
26. Diller E et al (2011) Control of multiple heterogeneous magnetic microrobots in two dimensions on nonspecialized surfaces. IEEE Trans Robot 28(1):172–182
27. Huang T-Y, Qiu F, Tung HW, Peyer KE, Shamsudhin N, Pokki J, Zhang L, Chen XB, Nelson BJ, Sakar MS (2014) Cooperative manipulation and transport of microobjects using multiple helical microcarriers. RSC Adv 4(51):26771–26776
28. Kei Cheang U, Lee K, Julius AA, Kim MJ (2014) Multiple-robot drug delivery strategy through coordinated teams of microswimmers. Appl Phys Lett 105(8):083705
29. Das S, Steager EB, Hsieh MA, Stebe KJ, Kumar V (2018) Experiments and open-loop control of multiple catalytic microrobots. Journal of Micro-Bio Robotics 14(1–2):25–34
30. Huang TY, Sakar MS, Mao A, Petruska AJ, Qiu F, Chen XB, Kennedy S, Mooney D, Nelson BJ (2015) 3D printed microtransporters: compound micromachines for spatiotemporally controlled delivery of therapeutic agents. Adv Mater 27(42):6644–6650
31. Gueron S, Levit-Gurevich K (1998) Computation of the internal forces in cilia: application to ciliary motion, the effects of viscosity, and cilia interactions. Biophys J 74(4):1658–1676